HEFAT2010
7th International Conference on Heat Transfer, Fluid Mechanics and Thermodynamics
19-21 July 2010
Antalya, Turkey

Numerical Investigation of Dual Secondary Injection for Thrust Vector Control

Mohammadi E.* and Toloei A.
*Author for correspondence
Department of Space Engineering, Faculty of New Technologies and Energy Engineering,
Shahid Beheshti University,
Tehran,
Iran,
E-mail: emohammadii@gamil.com

ABSTRACT

Dual secondary injection for thrust vectoring in a convergent-divergent nozzle is studied by solving three dimensional RANS equations with the help of a Computational Fluid Dynamics (CFD) code. This study surveys the flowfield structure and performance of dual secondary injection and compare with single secondary injection. Air as calorifically perfect gas is used for primary and secondary flows. Realizable k-ε (Rke) turbulent model with enhanced wall treatment approach is used for viscous model. Density based solver and explicit scheme are used as solver. A set of tests with different distance between ports are run to investigate the effect of injection location on the flowfield. Results stated that for the specified test nozzle and fix secondary mass flow rate dual injection with distance between two ports bigger than nearly 8.5 diameter of the injection port produces side force more than a single injection with the same mass flow rate. It also reduces the probability of bow shock impingement to the opposite wall and therefore side force production has less limitation.

INTRODUCTION

There are many subjects in aerospace and fluid mechanics engineering which have challenge with transverse injection into a supersonic flow such as boundary layer control, separation control, entry thermal protection and fuel injection. Secondary Injection for Thrust Vector Control (SITVC) is one of them. A flying vehicle propulsion system in addition to providing propulsive force can control vehicle's attitude and trajectory by changing thrust vector, i.e., changing the angel of the vector which normally assigned parallel to the vehicle. As far as vehicle's engine works TVC is useful and it does not depend on aerodynamic forces. So it is also useful in thin atmosphere and ultra-atmosphere where aerodynamic forces do not work. Moreover a fighter aircraft should have high agility, maneuverability and survivability which can not be provided by aerodynamic methods [1].

Different methods of TVC such as gimballed motors, movable nozzles, movable flaps and secondary injection are introduced. SITVC is based on changing the flowfield of diverging part of the nozzle. This was first recommended by A. E. Wetherbee in 1949 [1]. Secondary flow acts as an object in front of the supersonic primary flow and so a bow shock appears which makes a weak separation shock due to interaction with boundary layer upstream of the injection location. Boundary layer separation results pressure gradient on the nozzle walls. Momentum of the injectant and the pressure gradient produces a side force that can deflect the thrust vector of the nozzle. Jet and supersonic flow interaction phenomena depends on primary and secondary flow properties especially jet power, Mach number of primary flow and secondary flow properties. Since there are several problems with mechanical thrust vectoring, for instance, heavy mechanical hardware, which adds weight to the vehicle and increase nozzle complexity, adding to maintenance requirement and also since there is no mechanical hardware other than control valves in fluidic thrust vectoring [3], many experimental, theoretical and numerical studies have been accomplished in this field.

Due to complexity of secondary injection interaction with the primary flow theoretical models hold only for very low injection flow rates and lack generality [4]. Linearized model [5], Blast-wave analogy [6] and Boundary layer separation model [7] are some of the theoretical models which most of them are provide by experimental tests. Experimental tests are costly and provide only macroscopic performance estimations. Numerical studies supply precious results that can be a complementary element to experiments. Balu represents an inviscid model by claiming the insignificant effects of boundary layer on the side force [8]. Ko has presented a three dimensional viscous flow analysis of the secondary injection thrust vector control system for a conical rocket nozzle and employing two turbulence models, namely, algebraic Baldwin-Lomax model and two equation turbulence closure(k-ε) model with low Reynolds number treatment [9]. Erdem used commercial CFD code called Fluent for simulating the nozzle which is used by Ko and tested several solution parameters such as different turbulence models with distinct wall treatment

approaches, different computational grid sizes, types and solver types and compare with experimental results [10].

To improve SITVC performance some new techniques are introduced such as multiple injection which increases thrust vectoring capability without any thrust performance penalties [3]. Waithe [3] modelled a two dimensional nozzle with two slots in the diverging section and investigated the flowfield of the nozzle numerically and experimentally.

The present study aims at the investigation of the flowfield structure and performance of a dual injection nozzle and comparing with a single injection one with solving three dimensional Reynolds-Averaged Navier-Stokes (RANS) equations by a numerical approach using CFD code.

NOMENCLATURE

$y+$	[-]	non-dimensionalized distance from the wall
v	[Kg/m.s]	kinematic viscosity
u_τ	[-]	non-dimensionalized friction velocity
U_e	[m/s]	free stream velocity
C_f	[-]	skin friction coefficient
Re	[-]	Reynolds number
F_p	[N]	primary axial thrust
F_s	[N]	side thrust
F_n	[N]	interaction force
F_j	[N]	jet reaction force
ΔA_y	[m^2]	Y-face area of grid cell
$\dot{m}_s$	[kg/m^3]	secondary mass flow rate
$\dot{m}_p$	[kg/m^3]	primary mass flow rate
ge	[m/s^2]	gravitational acceleration
V_{sy}	[pa]	Y-component of secondary flow exit velocity
P_{es}	[pa]	secondary exit pressure at injection slot exit
P_{as}	[pa]	secondary ambient pressure at injection slot exit
A_s	[m^2]	injection slot area
β_{inj}	[-]	angle between normal to the wall at point of injection and the normal to the primary nozzle axis
D_i	[m]	diameter of injection slot
D_t	[m]	diameter of nozzle throat
Isp_s	[sec]	side specific impulse
Isp_{sys}	[sec]	system specific impulse

TEST CASE NOZZLE AND CONDITIONS

A three dimensional convergent-divergent nozzle with two circular ports on the divergent section is used (Fig.1). Dimensions are in millimetre. Each injection port diameter is 10 mm. The half geometry is modelled. The boundary conditions for the inlet and injection ports are summarized in Table 1.

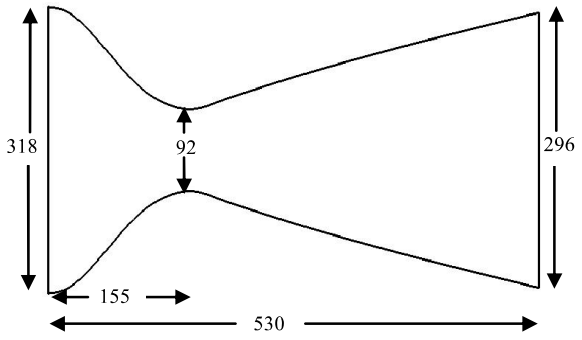

Figure 1 Geometry of the model

For nozzle inlet and injectant ports boundary conditions are pressure-inlet condition, for nozzle outlet boundary condition is outlet-pressure, for middle plane boundary condition is symmetry and for walls boundary condition is wall. Boundary condition settings of inlets have been set as depicted in Table 1. Injection is supposed to be normal to the wall. For outlet boundary condition atmospheric pressure and 300k temperature have been chosen. For turbulence specification method of inlet conditions, intensity and hydraulic diameter have been selected. According to Erdem [10] recommendations 5% for turbulent intensity of rocket nozzle and nozzle inlet radius for hydraulic diameter of half geometry is suitable.

Table 1 Primary and secondary flow conditions

	Mach #	Fluid	Total pressure	Total temperature
Nozzle Inlet	0.3	Air	6800(kpa)	2400(k)
Orifices	1	Air	6800(kpa)	2400(k)

SOLVER SETTINGS AND TURBULENCE MODELLING

Due to compressible flowfield, the explicit density based steady state solver has been chosen. The primary and secondary flows are air as a calorifically perfect gas. Realizable k-ε model with enhanced wall treatment has been selected for turbulence modelling as proposed by Erdem [10]. According to near wall treatment y+ criterion has to be less than 1. Maintaining the criteria it most select the right size for the first cell distance which is estimated using skin friction coefficient (Cf) formula for pipe flows [10]. It has to be noted that x in Rex is the distance from the inlet to injection port, in front of which boundary layer separates, and using the definitions of y+ and Uτ, first cell distance is found for the wall treatment approach as 2.7×10^{-4}mm as in Eq.(1).

$$y = \frac{y^+ \nu}{u_\tau} = \frac{y^+ \nu}{U_e \cdot \sqrt{C_f/2}} = \frac{y^+ \nu}{U_e \cdot \sqrt{0.046.\mathrm{Re}_x^{-0.2}}} \quad (1)$$

Table 2 shows the computational grid specifications used. Fig 2 shows y+ contours on nozzle wall which mostly satisfy the criteria. This is important for turbulence modelling.

Table 2 Computational grid specifications

Boundary layer height (mm)	0.149
Boundary layer grid first cell height (mm)	0.00027
Number of cells in boundary layer grid	30

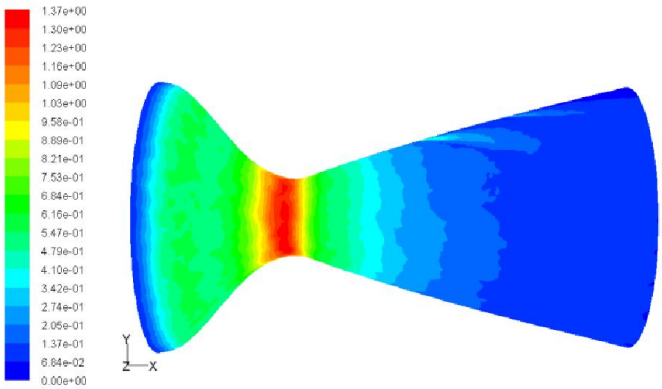

Figure 2 y+ contours on the nozzle (with RKE)

VERIFICATION OF THE SOLVER AND TURBULENCE MODEL

Verifying the solver settings and turbulence modelling, a three dimensional flat plate simulation with experimental results [11] is depicted in figure 3. Primary and secondary flow conditions are depicted in Table 3. Results show good settlement of numerical solution on experiments.

Table 3 Primary and secondary flow conditions used for flat plate simulation

	Fluid	Stagnation Temperature (k)	Stagnation Pressure (Pa)	Mach Number
Primary Flow	Air	300	48230	2.61
Secondary Flow	Nitrogen	300	48230	1

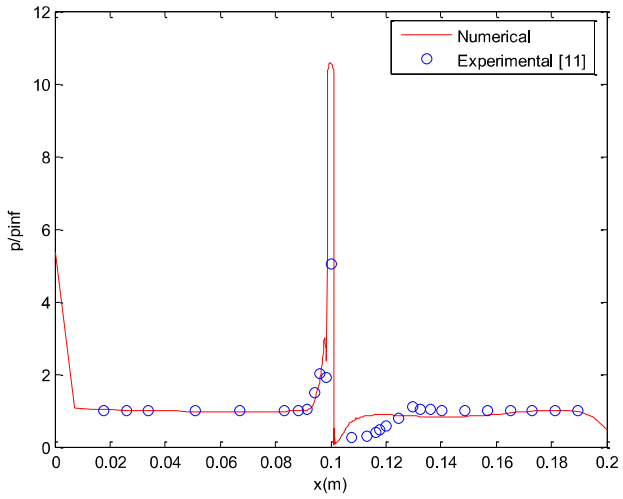

Figure 3 Numerical and experimental result comparisons for flat plate

COMPUTATIONAL GRID

The computational grid generated by a commercial grid generator for the half geometry and includes unstructured cells. Erdem [10] noted that the unstructured grid significantly lowers the mesh size and is computationally feasible.

Three distinct computational grids of 350388 nodes, 510701 nodes and 783331 nodes for this geometry are generated shown in figure 4. Despite refining the grids, the side and primary forces in the second and the third grids do not experience considerable changes shown in Table 4. Thus the second grid has been selected for analysis.

Table 4 Grid Dependency Results

Number of Nodes	F_p(N)	Fs(N)
350388	30600.87	703.2537
510701	30778.34	772.0674
783331	31273.31	770.7701

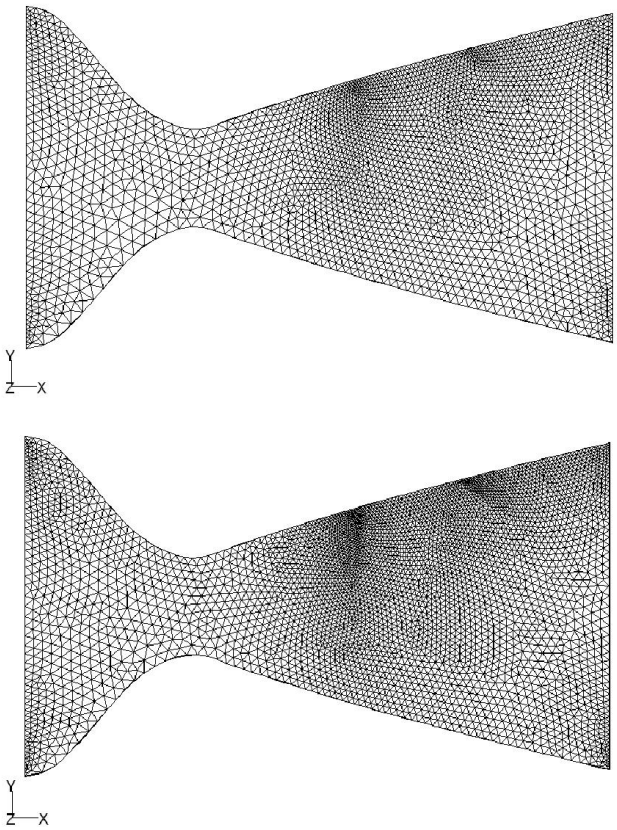

Figure 4 Grids on the symmetry plane corresponding to the three meshes used in grid dependency

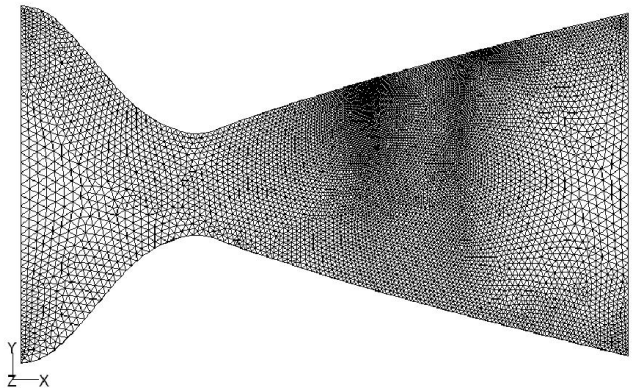

Figure 4 (continued) Grids on the symmetry plane corresponding to the three meshes used in grid dependency

FLOWFIELD STRUCTURES

Investigating the effect of injectant ports distance, it has been decided to have a fix location port and change the other ones. The fix port location determined correspondent to the optimum point according to Rezayii [12] research. As Rezayii concluded the non-dimensional length of x/D_t=4.4 is the location of maximum side force. Table 5 shows the second port locations in the tests.

Table 5 The second port distance to the fix port

Test Number	Distance to the fix port /Di
1	No Injection
2	15
3	12.5
4	10
5	7.5
6	5
7	2.5
8	0(single injection)

For symmetry plane of different injectant port locations comparison of Mach number contours (See Fig. 5) reveals:

- In test 1 which there is no injection, symmetrical mach number contours can be seen.
- In tests 2, 3 and 4 two distinct bow shocks appear. For each port two regions can be seen; upstream high pressure region and downstream low pressure region.
- In test 5 second port injects to the downstream low pressure region of the first one and so the upstream high pressure region of the second one and the downstream low pressure region of the first one interfere.
- In tests 6 and 7 the second injection are done almost inside the first downstream vortex. Just one bow shock appears.
- Test 8 is a single injection which has the mass flow rate equals to the sum of the mass flow rate of two ports of the other tests. Stronger bow shock (bigger shock angle) introduces in this test compare to test 6.
- No bow shock impingement, which is a common problem in single secondary injection in nozzles, occurred in all tests.

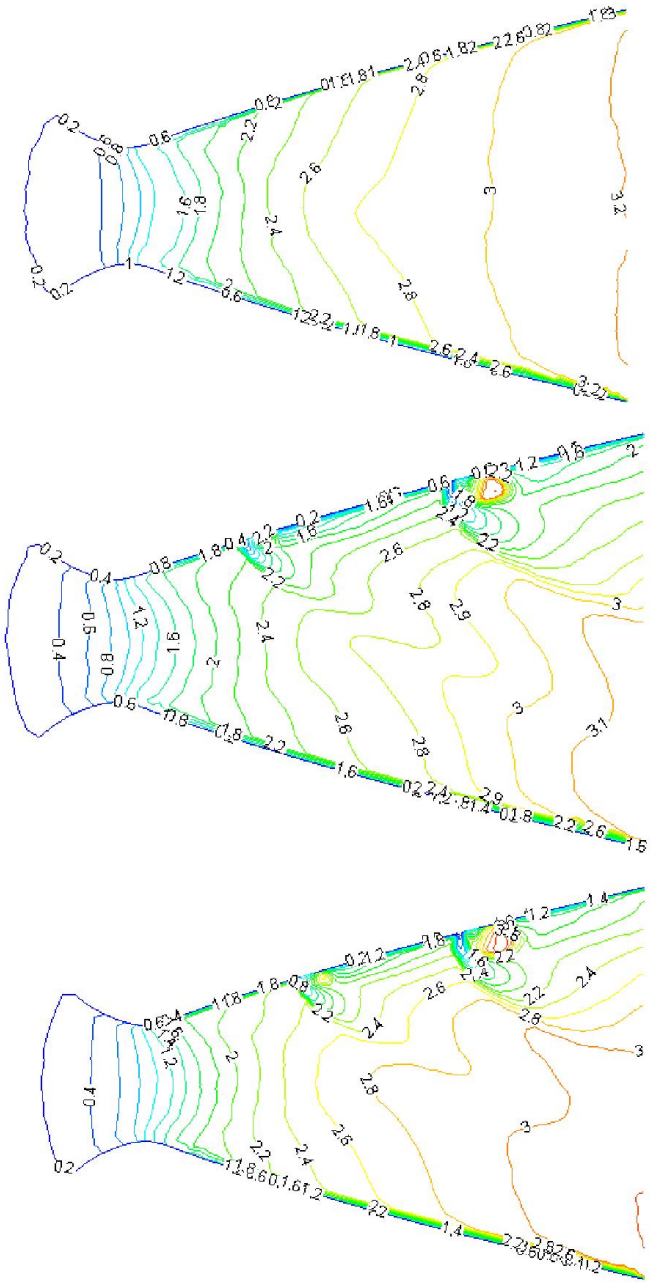

Figure 5 Mach number contours in symmetry plane

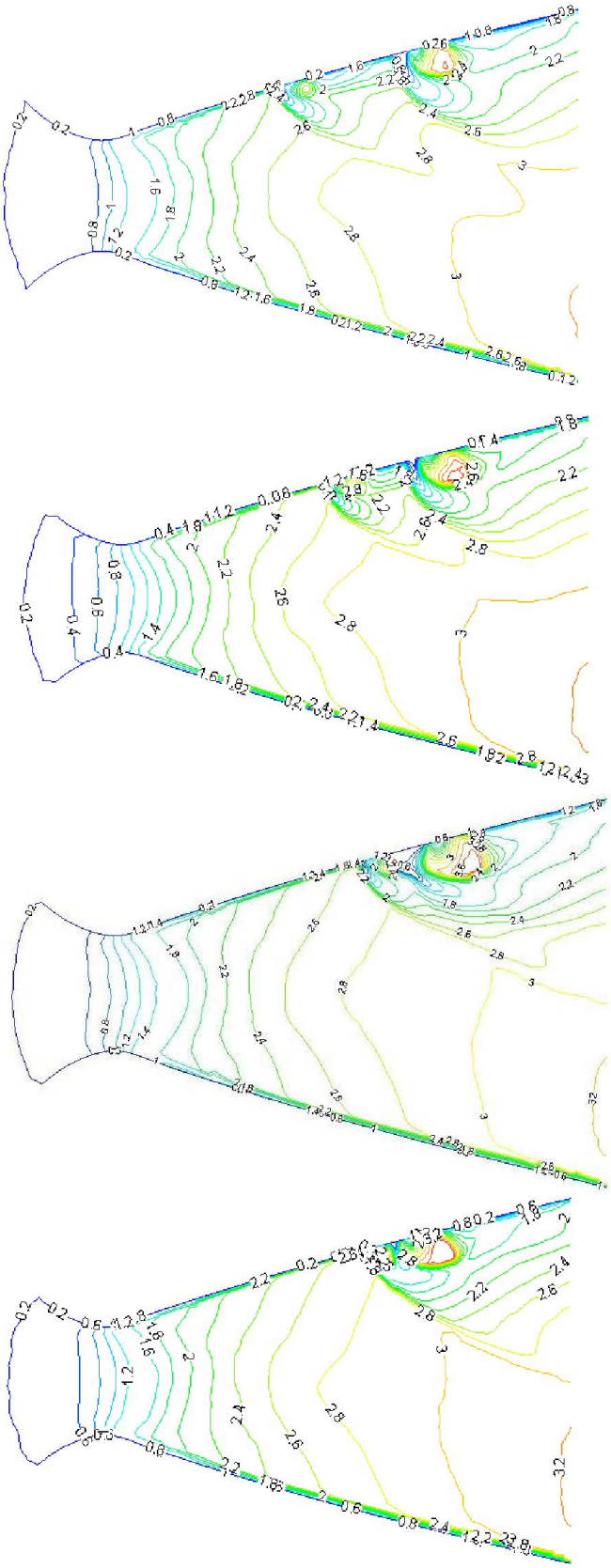

Figure 5 (continued) Mach number contours in symmetry plane

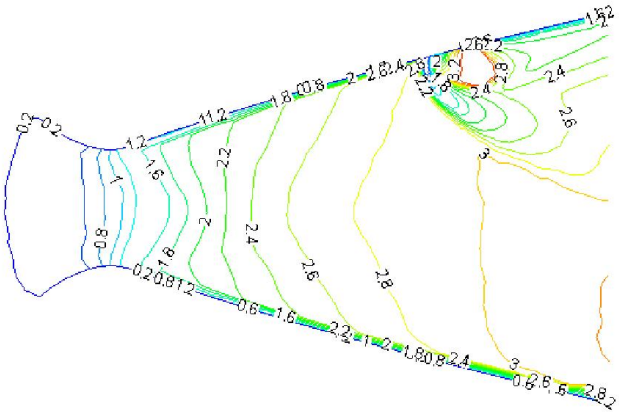

Figure 5 (continued) Mach number contours in symmetry plane

PERFORMANCE EVALUATION

This section involves the evaluation of the performance of dual secondary injection and the effect of injectant port distance. The side force consists of two parts; Interaction force and jet reaction force:

$$F_s = F_n + F_j \tag{2}$$

Interaction force is the pressure component of the side force which is due to pressure gradient in the wall:

$$F_n = \sum_i \left[P\Delta A_y\right]_{upper-wall} - \sum_i \left[P\Delta A_y\right]_{down-wall} \tag{3}$$

Jet reaction force is the momentum component of the side force and appears because of the momentum of the injectant:

$$F_j = \dot{m}_s V_{sy} + \left[(P_{es} - P_{as})A_s\right]\cos\beta_{inj} \tag{4}$$

Figure 6 shows the effects of injection ports distance on SITVC. Fig. 6 also shows the side force calculated by an analytical model introduced by Broadwell [6] named Blast Wave Analogy Model. The distance is non-dimensionalized by diameter of injectant port and forces are non-dimensionalized by non injection axial force (test1). Jet reaction force has no change with changing the distance but interaction force completely depends on the ports location. Side force changes corresponding to interaction force because of nearly fix value of jet reaction force. The test 8 which has single injection is depicted with zero value of the distance.

As it can be observed nozzles with near ports to the fix port make small interaction forces. In some tests it is even less than single injection (tests 5, 6, 7). Increasing the distance of the two injection ports, develops each injection regions, upstream high pressure region and downstream low pressure region, and makes more side force. In test 3 the maximum value of side force generates. In this test each injection has enough space to extend. In test 2 despite injection ports are far enough to extend completely, but the primary flow velocity when interacts with the first secondary flow is less than the test 3 so the pressure rise after the bow shock is less than test 3 and therefore the upstream higher pressure is weaker than the test 3 and so in test 2 less side force produces.

Side force corresponding to analytical model does not change due to injection locations because the model is designed for conditions which every injection works independently and

so no dissipation and interaction of two injections is considered. The analytical and numerical solutions close most in test 3 which the best interaction between secondary flow and shock wave happens and dissipation is the least. Since the analytical model treated the flow as inviscid flow and limited to two dimension analysis over predicts in all cases.

Side specific impulse and system specific Impulse are defined as following:

$$Isp_s = \frac{F_s}{\dot{m}_s g_e} \tag{5}$$

$$Isp_{sys} = \frac{\sqrt{F_p^2 + F_s^2}}{(\dot{m}_p + \dot{m}_s) g_e} \tag{6}$$

In Figure 7 Side specific Impulse and system specific impulse are non-dimensionalized by specific impulse of the non injection test (Test 1). Side specific impulse (Isp_s) changes like side force but system specific impulse (Isp_{sys}) is mostly fixed. The main reason is that all of the changes are small compare to primary thrust value (F_p).

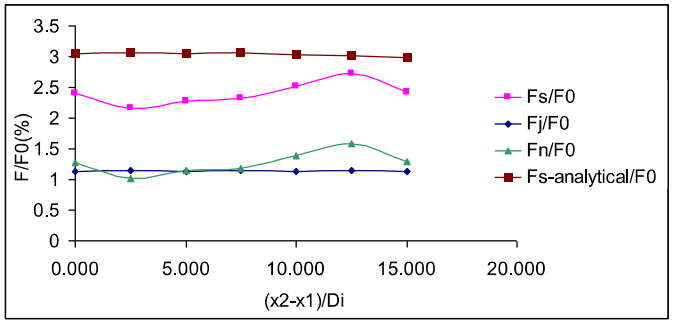

Figure 6 Secondary injection forces

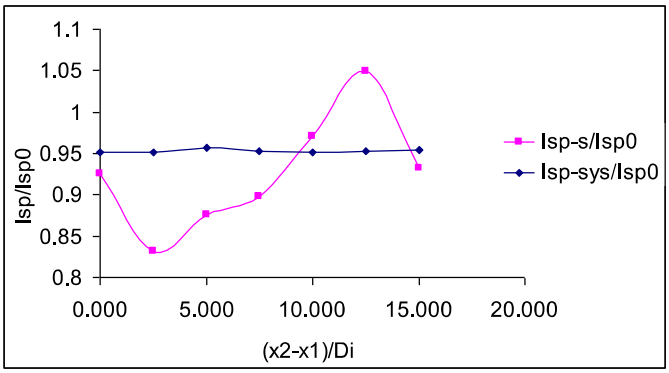

Figure 7 Side and system specific impulses

CONCLUSION

Comparison of dual secondary injection performance and structure with usual secondary injection thrust vector control systems for the same secondary flow conditions is studied in this survey with the help of a CFD code. The effects of distance between two injection ports on Flowfield structure and SITVC performance also investigated. The results stated that for the specified test nozzle and fix secondary mass flow rate dual injection with distance between two ports bigger than nearly 8.5 diameter of the injection port produces the side force more than a single injection with the same mass flow rate. Two important benefits of dual secondary injection which resulted in this study are as follows:

Dual secondary injection produces specified value of side force with less mass flow rate if the distance of two injections be in the definite limitations.

As mentioned by the others [10, 12, 13] one of the most important problems in single secondary injection systems is the bow shock impingement to the nozzle opposite wall which decreases the side force and since the phenomena probability increases with mass flow rate increasing, there is mass flow rate limitation and therefore there is limitation in side force generation. Since in dual secondary injection with less mass flow rate for two injectant ports and half for each port can reach the same side force, the probability of shock impingement reduces and so there would be less limitation on side force generation.

ACKNOWLEDGEMENT

We would like to express our deep gratitude to Mr. Erinc Erdem, Mr. Mohsaen Nazari and Mr. Ali Shia Nezhad Hesar for their guidance in this research.

REFERENCES

[1] Sutton, G. P.; Biblarz, O.: Rocket Propulsion Elements, John Willey & Sons, 2001.

[2] Ghasemi, H., Firoozabadi, B., Rezayi, H.: Simulation of lateral interaction with flat plate flow, Fluid dynamics Conf., Tabriz University, 2003.iversity, 2003.

[3] Waithe, K. A.; Deere, K. A.: Experimental and Computational Investigation of Multiple Injection Ports in a Convergent-Divergent Nozzle for Fluidic Thrust Vectoring, AIAA 2003-3802, June 2003.

[4] Erdem, E.; Albayrak, K.; Tinaztepe, H. T.: Parametric Study of Secondary Gas Injection into a Conical Rocket Nozzle for Thrust Vectoring, AIAA 2006-4942, July 2006.

[5] Walker, R. E.; Shandor, M.: Influence of Injection Properties for Fluid-Injection Thrust Vector Control, J. Spacecraft, Vol.1 No. 4, July-August 1964, pp. 409-413.

[6] Broadwell, J. E., Analysis of Fluid Mechanics of Secondary Injection for Thrust
Vector Control, AIAA Journal, Vol. 1, No. 10, 1963, pp. 580–585.

[7] Wu, J. M., Chapkis, R. L., and Mager, A., Approximate Analysis of Thrust Vector Control by Fluid Injection, ARS Journal, Vol. 31, No. 6, Dec. 1961, pp. 1677–1685.

[8] Balu, R., Analysis of Performance of a Hot Gas Injection Thrust Vector Control
System, Journal of Propulsion and Power, Vol. 7, No. 4, 1991, pp. 580–585.

[9]Ko, Hyun and Yoon, Woong-Sup, Performance Analysis of Secondary Gas Injection into a Conical Rocket Nozzle, Journal of Propulsion and Power, Vol. 18 No. 3, May-June 2002.

[10] Erdem, E.; Albayrak, K.; Tinaztepe, H. T.: Numerical Investigation of Flowfield Inside a Conical Rocket Nozzle in the Presence of Transverse Injection, AIAA 2008-359, January 2008.

[11] Zukoski, E. E., and Spaid, F. W., Secondary Injection of Gases into a Supersonic Flow, AIAA journal, Vol. 2, No. 10, October 1964, pp. 1689-1696.

[12] Rezayii, H.: Nozzle Flowfield Simulation with Secondary Injection for Thrust Vector Control (SITVC), Master of Science Thesis, Sharif University of Technology, 2003.

[13] Sadiq, M. U.; Performance Analysis and Flowfield Characterization of Secondary Injection Thrust Vector Control For a 2DCD Nozzle, Master of Science Thesis, August 2007.